EARTH SURFACE PROCESSES AND LANDFORMS
Earth Surf. Process. Landforms **42**, 1549–1559 (2017)

Published online 19 February 2017 in Wiley Online Library
(wileyonlinelibrary.com) DOI: 10.1002/esp.4112

Terrain attributes of earthquake- and rainstorm-induced landslides in orogenic mountain Belt, Taiwan

Jr-Chuan Huang,[1]* John D. Milliman,[2] Tsung-Yu Lee,[3] Yi-Chin Chen,[4] Jiin-Fa Lee,[5] Cheng-Chien Liu,[6] Jiun-Chuan Lin[1] and Shuh-Ji Kao[7]

[1] Department of Geography, National Taiwan University, Taipei, Taiwan
[2] Virginia Institute of Marine Science, College of William and Mary, Williamsburg, VA USA
[3] Department of Geography, National Taiwan Normal University, Taipei, Taiwan
[4] Department of Geography, National Changhua University of Education, Changhua, Taiwan
[5] Central Geological Survey, MOEA, Taipei, Taiwan
[6] Department of Earth Science, National Cheng-Kung University, Tainan, Taiwan
[7] State Key Laboratory of Marine Environmental Science, Xiamen University, Xiamen, China

Received 12 February 2016; Revised 12 January 2017; Accepted 16 January 2017

*Correspondence to: Jr-Chuan Huang, Department of Geography, National Taiwan University, Taipei 106, Taiwan. E-mail: riverhuang@ntu.edu.tw

ESPL
Earth Surface Processes and Landforms

ABSTRACT: Landsliding induced by earthquakes and rainstorms in montane regions is not only a sculptor for shaping the landscape, but also a driver for delivering sediments and above-ground biomass downstream. However, the terrain attributes of earthquake- and rainstorm-induced landslides are less discussed comprehensively in Taiwan. As part of an island-wide inventory, we here compare and contrast the landslide terrain attributes resulting from two catastrophic events: the Chi-Chi earthquake ($M_w = 7.6$, September 1999) and typhoon Morakot (rainfall >2500 mm, August 2009). Results show that the earthquake-induced landslides are relatively small, round-shaped and prone to occur primarily in middle and toe of slopes. In contrast, the rainstorm-induced landslides are larger, horseshoe-shaped and preferentially occurring in slope toes. Also, earthquake-induced landslides, particularly large landslides, are usually found at steeper gradients, whereas rainstorm-induced landslides aggregate at gradients between 25° and 40°. Lithologic control plays a secondary role in landsliding. From an island-wide perspective, high landslide density locates in the region of earthquake intensity ≥ VI or one-day rainfall ≥600 mm day^{-1}. Through the landslide patterns and their terrain attributes, our retrospective approach sheds light on accessing the historical and remote events for close geophysical investigations. Finally, we should bear in mind that the landslide location, size, and terrain attributes varying with triggers may affect the landscape evaluation or biogeochemical processes in landslide-dominated regions. Copyright © 2017 John Wiley & Sons, Ltd.

KEYWORDS: landslides; earthquake; typhoon; Taiwan

Introduction

Landslides triggered by earthquakes and rainstorms in montane and orogenic regions dominate mass wasting (Hovius *et al.*, 2000; Dadson *et al.*, 2004; Kao and Milliman, 2008) as well as induce devastating hazards that threaten both property and life (Huang and Kao, 2006; Kao *et al.*, 2011). Massive flux of eroded terrestrial sediment and woody debris not only sculpture the landscape (Montgomery and Brandon, 2002; Korup 2005a; Larsen *et al.*, 2010; Gao and Maro, 2010), but also spike biochemical cycling (Hilton *et al.*, 2008; Hilton *et al.*, 2011; West *et al.*, 2011). Massive landslides also expose new, fresh rocks to enhance chemical weathering which consumes the carbon dioxide in the atmosphere and then regulates the carbon cycle and global climate. Thus, the response of landsliding to different triggers on terrain attributes should be clarified (Wu and Chen, 2009).

Previous studies have demonstrated that the location and size of landslides induced by earthquakes and rainstorms may differ (Lin *et al.*, 2006; Huang and Montgomery, 2014). Hypothetically, the earthquake- and rainstorm-induced landslides tend to occur in upper and lower hillslopes, respectively (Densmore and Hovius, 2000). Earthquake-induced landslides are primarily governed by the interaction of seismic waves and topography; thus landslides occur along ridgetops. In contrast, the rainstorm-induced landslides are frequently found in the slope toes due to greater degree of soil water saturation (Montgomery and Dietrich, 1994; Huang *et al.*, 2007). However, some studies in central Taiwan did not show such a clear pattern (Lin *et al.*, 2006; Meunier *et al.*, 2008). The failure to identify the pattern may be attributed to landslide fingerprints being imprinted by consequent events or the study area being not sufficiently large enough. This hypothesis needs to be clarified if we are to better understand landscape evolution in

landslide-dominant regions. Meanwhile, the correlations between different triggers and terrain attributes of landslides are rarely discussed. The correlations might be of use for investigating historical events retrospectively.

Taiwan, located at the juncture between the Philippine and Eurasian tectonic plates and also in the path of tropical cyclones, is a hotspot for landsliding induced by both earthquake and typhoon and thus high rates of erosion and sediment transport were well-documented (e.g. Dadson *et al.*, 2003; Milliman *et al.*, 2007; Lin *et al.*, 2008; Chen *et al.*, 2013). It is not coincidental that eight of the 13 documented highest sediment-yield rivers in the world are located in Taiwan (Milliman and Farnsworth, 2011). In recent years, two extreme catastrophes occurred in Taiwan: the Chi-Chi earthquake ($M_w = 7.6$, September 21, 1999) and Typhoon Morakot (brought as much as 2750 mm of rainfall locally, August 7–9, 2009). Both events resulted in massive island-wide landslides. The Chi-Chi earthquake, the largest earthquake (in the history of observation) striking central Taiwan in the last century, caused numerous landslides that left massive landslide deposits (Chen *et al.*, 2006; Wu and Chen, 2009), many of which were flushed out during subsequent typhoons (Dadson *et al.*, 2004; Milliman *et al.*, 2007; Hovius *et al.*, 2011). The other catastrophic event, Typhoon Morakot, the most severe typhoon during the past five decades, brought over 2000 mm of rainfall in southern Taiwan (Tsai *et al.*, 2010; Tsou *et al.*, 2011; Chen *et al.*, 2013) and also induced massive landslides. Utilizing island-wide landslide inventories triggered by various forcing intensities provide us with an ideal chance to differentiate the terrain attributes between earthquake- and rainstorm-induced landslides. This study analyzed the two island-wide landslide inventories through correlating the inventories with the terrain attributes of landslides: namely, elevation, slope, rock type, and position at hillslope. The examination of these terrain attributes with different drivers and forcing intensity can not only test the hypothesis of landslide location, but also determine the sensitivities of environmental settings to landslides.

Environmental Setting of Taiwan

Taiwan's landscape is the result of the ongoing oblique collision between the Philippine Sea Plate and the Asian continent with uplift rates ranging 4 to 10 mm yr^{-1} (Chai, 1972; Ho, 1988; Teng, 1990). This active orogenic collision has formed the central mountain range with many summits higher than 3000 m and a correspondingly rugged and steep terrain (Figure 1a). About two-thirds of Taiwan lies at higher than 100 m, and slopes with gradient >30° account for 58% of the total land area (Figure 1b).

Geologically, the island has five distinct topographic zones and eight basic rock types (Figure 1c). From east to west the topographic zones are:

1 The Eastern Coastal Range is a small and narrow mountain range with elevations less than 1500 m. Rocks consist entirely of Luzon arc-related volcanic (andesite) and sedimentary (sandstone) rocks (Teng, 1990).
2 The north–south oriented Central Range is the backbone of the island, with steep topography and many summits higher than 3000 m. A greenschist to amphibolite facies, related to the Tananao Metamorphic Complex, is wide spread. The metamorphic rocks, such as phyllite, slate, and schist with sandstone interbeds, are common.
3 The Hsueshan Range, located in the north, consists of Eocene and Miocene metamorphic rocks, mainly argillite, and quartzites with intercalated shale and sandstone. Elevations tend to be above 2000 m and locally exceed 3000 m with gradients commonly >30°.
4 The hilly Western Foothills Fold-thrust Belt, with 100–1500 m elevations, consists of thick sedimentary rocks composed by sandstone, mudstone, and shale. Those riverine and offshore marine sediments interbedded with alluvial-fan gravels are derived from the Central Range. Clay content increases to the south; mudstone badlands and mud volcanoes are not uncommon. The mud dominance results in much higher sediment concentrations in southern rivers, particularly the Choshui, Tsengwen and Erhjen Rivers (Kao and Milliman, 2008).
5 The Western Fluvial Plain is composed of fluvial sand/mud eroded from the Western Foothills. Elevations are less than 100 m with low gradients. These 12 000 km^2 (~30% of the island) of fluvial fans sustain most of Taiwan's agricultural activities and house most of the island's inhabitants.

Earthquakes and Typhoons in Taiwan

Both earthquakes and typhoons vary considerably in both of time and space, the intensities generally decreasing with the distance from the event's epicenter. Earthquakes in eastern Taiwan tend to be more frequent and depth-seated due to continent-arc

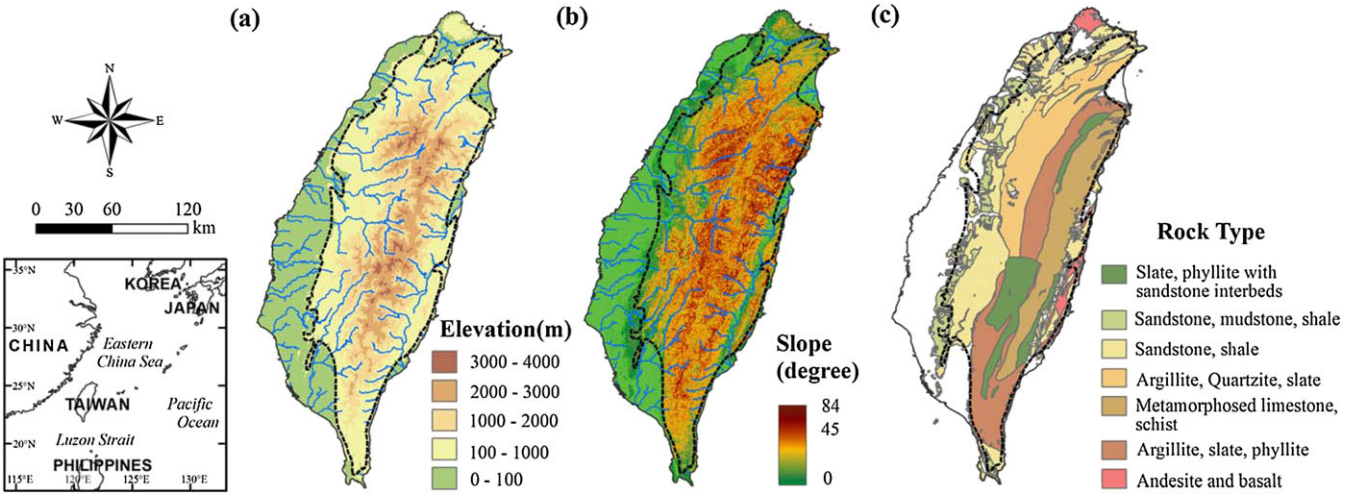

Figure 1. Topographic relief map of Taiwan showing the elevation distribution (a), the slope distribution (b) indicating the steepness of Taiwan and the lithologic units of Taiwan (c). [Colour figure can be viewed at wileyonlinelibrary.com]

collision, but are less destructive. Between 1999 and 2009, Taiwan had five earthquakes with earthquake magnitude $M_w \geq 6$ (Table I), the best-known being the Chi-Chi earthquake (September 21, 1999) and its major aftershock (October 22, 1999) in central Taiwan; both earthquakes affected the Hsueshan Range and the Central Range as well as the Taipei and Ilan basin in northern Taiwan (Figure 2a). The area with earthquake intensity ≥ VI (ground acceleration ≥ 250 gal) was larger than 1000 km^2, but its overall impact affected over 7000 km^2, ~ one-third of the mountainous area. In contrast, epicenters of the other three earthquakes were offshore, two in the east and one in the south; however, the areas with earthquake intensity ≥ VI were less than 400 km^2. Thus, only the Chi-Chi earthquake is used for representing the earthquake driver.

For rainstorms, annual precipitation in Taiwan averages ~2500 mm but is highly seasonal, with ~70% falling from May to October. There are three major types of rainfall in the wet season: (1) Mei-Yu, the frontal rainfall occurs in May and June, characterized by low intensity over a large area; it usually triggers few landslides; (2) in contrast, convective rainstorms tend to have high intensity but are limited in area and duration; (3) typhoon rainfalls are often intensive, wider in extent, and have longer duration (1–4 days). During 2006–2010, Taiwan experienced 19 typhoons (Table II), the radius of the typhoon centers ranging from 100 to 300 km; maximum one-day rainfall varied from 210 to 2700 mm day^{-1}. We used the island's 525 rain gauges to interpolate the island's maximum daily rainfall intensities instead of the maximum of rolling 24-hour rainfall intensity via the inverse distance weighted method (Figure 2 b), because hourly rainfall is not available for all rain gauges. As seen in Figure 2b, there was one distinct oval-shaped heavy rainfall area (area with >800 mm day^{-1} in Figure 2b), lying in mountainous southern Taiwan. Rainfall in the western fluvial plain of the island is relatively low.

Landslide Mapping

After Chi-Chi earthquake, the Central Geological Survey, MOEA of Taiwan's government, began to systematically initiate a long-term national dataset of landslides and debris flows. The Environmental & Engineering Division utilized the ortho-aerial photographs and satellite imagery from SPOT-2 or SPOT-4 (10 m spatial resolution) to manually delineate the landslides. These suspected landslides were compared to topographic maps and surface reflectivity from paired satellite images taken before and after the earthquake to determine the landslides induced by Chi-Chi earthquake; old or inactive landslides before

Table I. Extreme earthquakes during 1992–2009

Name	Date	Epicenter			Magnitude (M_w)	Area of intensity ≥ VI (km^2)
		Depth (km)	Longitude	Latitude		
Chi-Chi	September 21, 1999	8.0	120.82	23.85	7.6	7140
	October 22, 1999	12.1	120.40	23.51	6.4	1588
Chiayi	March 31, 2002	9.6	122.17	24.24	6.8	81
Taitung	April 1, 2006	7.2	121.08	22.88	6.2	379
Hengchuen	December 26, 2006	44.1	120.56	21.69	7.0	130

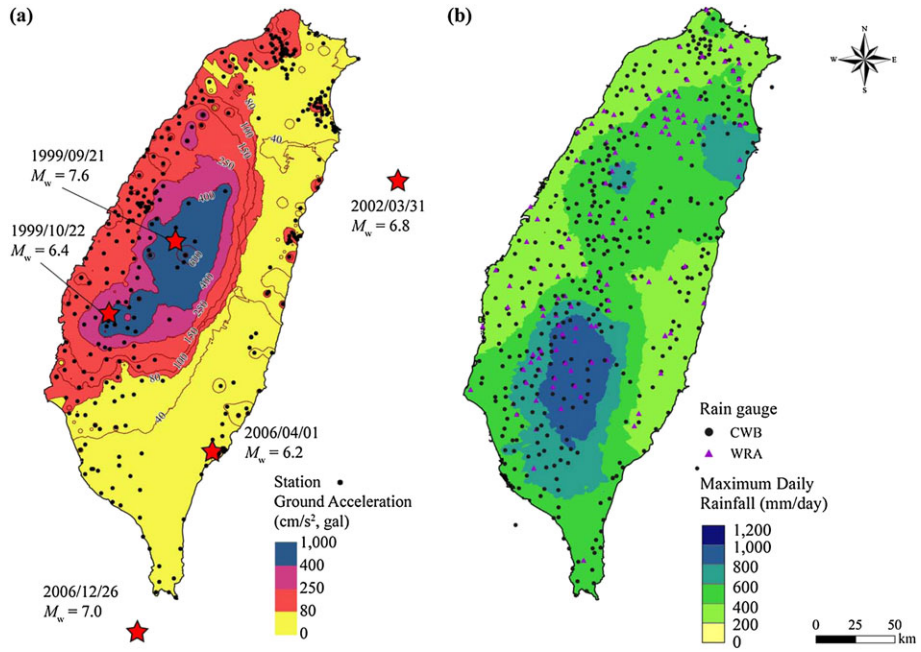

Figure 2. Ground acceleration distribution of Chi-Chi earthquake and the major aftershock (a) and the maximum one-day precipitation during 2006–2010 (b). In (a), the red star symbols represents the epicenters of the five extreme earthquakes during 1999–2010 and the black dots are the TSMIP network (Taiwan Strong Motion Instrumentation Program). The ground acceleration was interpolated from the 377 ground acceleration stations by the inverse distance weighted method (the power parameter is 0.5). In (b), the black dots are the 525 rain gauges including 394 from CWB (Central Weather Bureau) and 131 from WRA (Water Resources Agency). The maximum one-day precipitation was interpolated by using the inverse distance weighted method (the power parameter is 0.5). [Colour figure can be viewed at wileyonlinelibrary.com]

Table II. Extreme typhoons during 2006–2010

Typhoon	Date	Minimum pressure (hPa)	Radius of 15 m s^{-1} (km)	Maximum one-day rainfall (mm day^{-1})	Longitude	Latitude	Location[a]
Chanchu	May 16–18, 2006	943	300	207	121.2	23.12	eastern
Bilis	July 12–15, 2006	978	300	585	120.53	22.75	southern
Kaemi	July 23–26, 2006	960	200	259	121.3	22.97	eastern
Shanshan	September 14–16, 2006	945	200	217	121.18	24.49	central
Pabuk	August 6–8, 2007	980	150	375	120.74	22.01	southern
Sepat	August 16–19, 2007	920	250	868	121.49	24.18	eastern
Wipha	September 17–19, 2007	935	200	668	121.07	24.58	northern
Krosa	October 4–7, 2007	925	300	731	121.28	24.72	northern
Mitag	November 26–27, 2007	955	200	372	121.37	23.67	eastern
Kalmaegi	July 16–18, 2008	970	120	598	120.73	24.17	central
Fung-Wong	July 26–29, 2008	948	220	531	121.4	23.81	eastern
Sinlaku	September 11–16, 2008	925	250	880	120.99	24.27	central
Jangmi	September 26–29, 2008	925	280	901	121.52	24.51	northern
Morakot	August 5–10, 2009	955	250	1402	120.67	22.82	southern
Parma	October 3–6, 2009	945	250	1087	121.67	24.58	northern
Lionrock	August 31–September 2, 2010	990	100	338	121.04	22.92	eastern
Meranti	September 9–10, 2010	990	100	373	121	22.69	eastern
Fanapi	September 17–20, 2010	940	200	872	120.29	22.76	southern
Megi	October 21–23, 2010	935	250	716	121.83	24.52	northern

[a]Location indicates the maximum rainfall location in Taiwan.

the earthquake were precluded. In order to improve the accuracy of the landslide database, over 4000 accessible landslides were confirmed by investigation crews *in situ* for validation. The island-wide landslide inventory was released later on in 2002. Here, we used this landslide inventory to represent the landslides triggered by Chi-Chi earthquake.

For typhoon Morakot, the Forestry Bureau used the Export Landslide and Shaded Area Delineation System (ELSADS) to create an island-wide landslide map. This semi-automatic system for landslide delineation from satellite images uses the rectificated FORMOSA-2 imagery (with 2-m resolution), from which Normalized Difference Vegetation Index (NDVI) or Green Vegetation Index (GVI) can be used for landslide delineation (Liu *et al.*, 2011). Pre-determined landslide sites were also checked through overlaying the boundaries of those areas on the locally-enhanced image and digital terrain model (DTM) at a 1:5000 scale. To prevent the misinterpretation of cultivation, river, roads, the suspected landslides have been confirmed with topographic and land-use maps, and the misinterpreted features were manually removed. The two island-wide landslide maps produced by MOEA and Forestry Bureau thus provide valuable historical records in terms of integrity, though no landslide map created through remote sensing is perfect (Malamud *et al.*, 2004; Mondini *et al.*, 2011). For terrain attributes, the grid-based DTM with 40-m resolution was introduced for quantifying the terrain attributes of landslides. Considering the limitation of DTM resolution and the fact that the two landslide maps were derived from different sources, only landslide area $>1600\,m^2$ were selected and calculated the corresponded terrain attributes.

The landslide patterns of the Chi-Chi earthquake and Typhoon Morakot, respectively, are shown in Figures 3a and 3b.

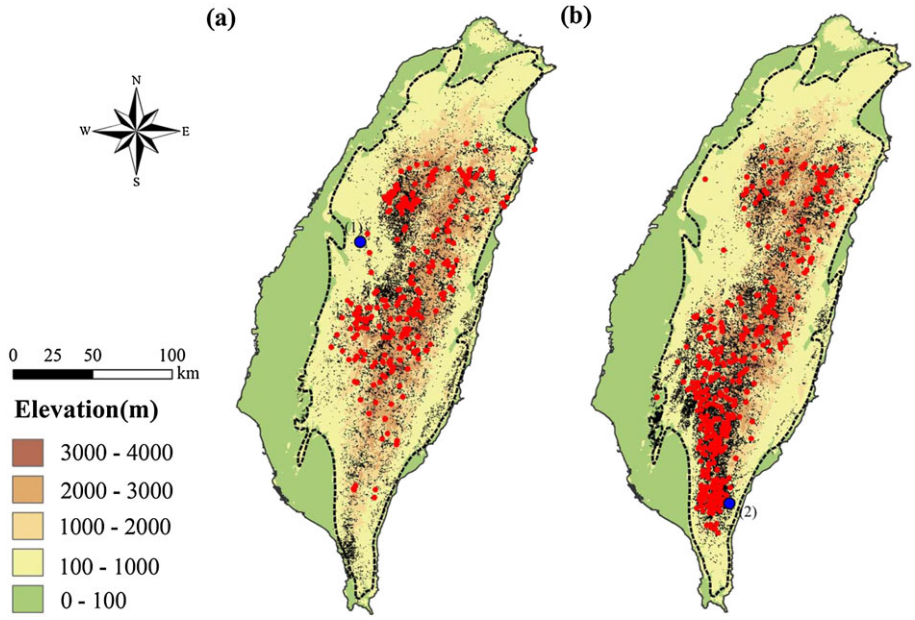

Figure 3. Landslide distributions induced by Chi-Chi earthquake (a) and Typhoon Morakot (b). The largest 1% landslides were marked by red dots. The blue circles indicated the locations of the landslides in 99 peaks (1) and landslides in Taimali (2) shown in Figure 10. [Colour figure can be viewed at wileyonlinelibrary.com]

The total landslide area by Morakot (583 km^2) is larger than that by Chi-Chi (419 km^2). Both of the largest 1% landslides (the red dots) aggregate mostly in central and southern Taiwan, corresponding closely to the epicenter of drivers. Besides, the landslides often spread over areas higher than 100 m in elevation, where they become the sources providing sediment to the rivers (Milliman *et al*., 2007).

Landslide Occurrence and Forcing Intensity

We firstly overlaid the earthquake intensity onto the Chi-Chi and Morakot landslide map to identify the correlation of earthquake intensity and the residual signal of Chi-Chi earthquake on Morakot landslide map (Figures 4a and 4b). In Figure 4, the proportional ratio, defined as the area of the specific condition (e.g. earthquake intensity or daily rainfall) over the total island area (elevation >100 m), was introduced to represent the background. Similarly, the landslide proportion ratio which is defined as the landslide area within the specific condition over the total landslide area is used for comparison with the background. From the perspective of stochastic process, the landslide proportion ratio should approximate the background, if the landsliding has no preference or occurs randomly. In contrast with random process, the landslide proportion ratio higher than background indicates the preference of landsliding in such a condition. Note that all the landslides were separated into two groups (i.e. the small and large landslides) to investigate the landsliding preference in terms of landslide size. In Figure 4a, areas stricken by earthquake intensity = VI and VII account for 15 and 20%, respectively, of the island, and areas affected by earthquake intensity ≥ V account for approximately 85% of the island. Thus the Chi-Chi earthquake definitely affected the entire island. For landslide area, the landslide proportion ratios (for both small and large landslides) within earthquake intensity = VI and VII are much higher than the background values. However, the landslide proportion ratios within earthquake intensity = IV and V are similar or slightly lower than background values, respectively. Comparing the landslide proportion ratios with the backgrounds, the landslide preference is increasing with the increase of earthquake intensity. Although we cannot affirm that landslides affected by earthquake intensity = V significantly, earthquake intensity scale = VI may well deserve a limit of catastrophic earthquake-induced landsliding. We further superimposed the earthquake intensity map onto the Morakot landslide map (Figure 4b). In this histogram, the landslide distribution does not show the preference tendency with the increase of earthquake intensity, indicating the irrelevancy between landslide map by Morakot and the Chi-Chi earthquake. It is not surprising because the landslides usually take 4–6 years to re-vegetate in Taiwan (Huang *et al*., 2006; Lin *et al*., 2004; Lin *et al*., 2005). Another reason is that the prior landslides before Typhoon Morakot have been excluded in the Morakot landslide map. Therefore, the residual signal of the Chi-Chi earthquake cannot significantly influence the landslide pattern 10 years later. We also superimposed the maximum one-day rainfall onto the landslides by Morakot to show the effect of corresponding rainfall on landslide distribution in Figure 5. In this histogram, the landslide preference occurs as the rainfall exceeds 600 mm day^{-1}. Rainfalls less than 400 mm day^{-1}, however, have little effect on triggering landslides; thus, rainfall >600 mm day^{-1} must cause numerous landslides island-wide. In summary, our investigation indicated that the landslides by the Chi-Chi earthquake mainly occurred in the area of earthquake intensity ≥ VI and the landslides by Morakot showed a preference in the areas of daily rainfall exceeding 600 mm day^{-1}. Meanwhile, no significant difference of landslide proportion ratios can be found in terms of landslide size.

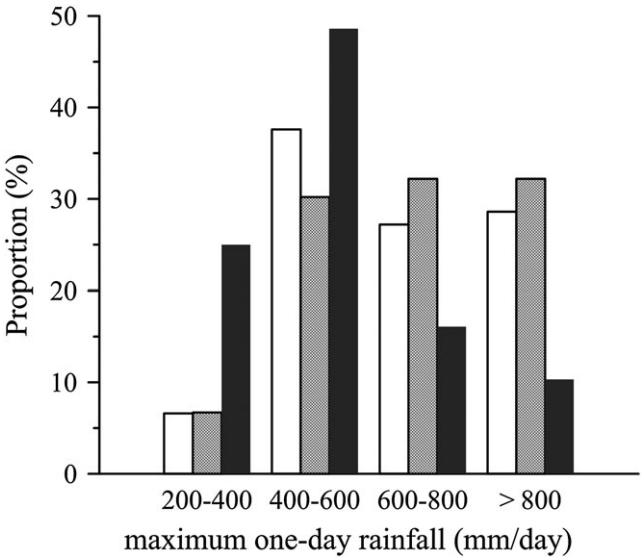

Figure 5. Landslide area fraction histograms for Morakot in the different maximum one-day rainfall regions (the maximum one-day rainfall was selected from 2006 to 2010, see text). The gray, white, and dashed bars indicated the whole area, small landslides, and large landslides, respectively.

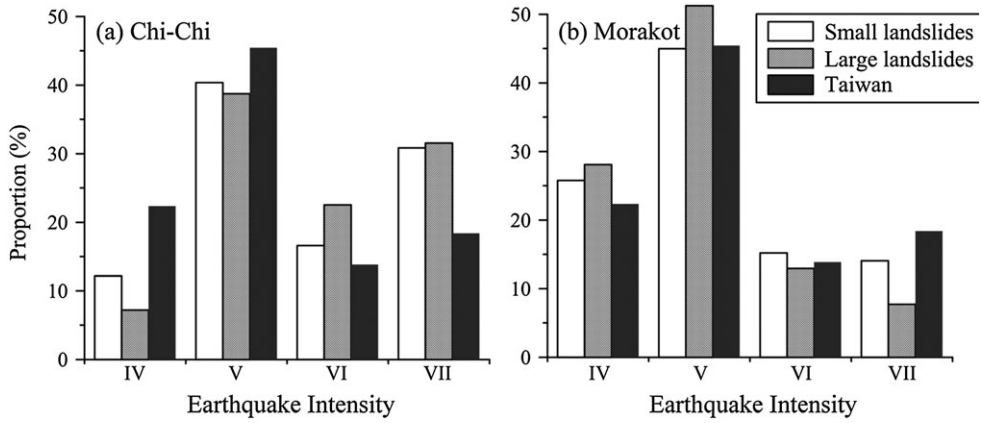

Figure 4. Landslide area fraction histograms for Chi-Chi earthquake (a) and Typhoon Morakot (b) comparing the area fraction of Chi-Chi earthquake intensity. The black bar represents the earthquake area proportion over whole Taiwan (elevation >100 m), the white and gray bars represent the small and large landslides, respectively. Note that the small and large landslides were separated by the equal total landslide area (see Table III).

A further scrutiny on small and large landslides was carried out by relating the landslide sizes with area and a shape attribute, the circumference ratio (R_{cir}), to identify the characteristics of landslide scars. The R_{cir} is defined as a ratio of landslide area over the area of a theoretical circle with the same perimeter of the landslide (Apaydin *et al*., 2006). Since the circle has the largest area as giving the same perimeter in geometry, this index ranges from 0.0 to 1.0, to approximate a circle. Table III illustrates the area, number, and shape index (R_{cir}) of the earthquake- and rainstorm-induced landslides. In general, the total landslide areas by Chi-Chi and Morakot are 419 and 583 km^2, around 2.1 and 2.8% of the entire island (only elevation >100 m was counted). The average area and total number of landslide triggered by the two events are 0.0165/0.0205 km^2 and 25337/28452, respectively (Table III). Only 4.8% of the landslide number can account for 50% of the total landslide area, indicating the rainstorm-induced landslides were relatively large and have large variation in terms of size (Table III). As for the landslide shape, the average of R_{cir} values for the earthquake-induced landslides were 0.43–0.58, suggesting that the small landslides are moderately circular than large ones. It is also the case for small typhoon-induced landslides. However, the average R_{cir} value for large landslides by Morakot was 0.24, indicating typhoon-induced landslide scars were not as circular as those by earthquake. The large landslides triggered by heavy rainstorms were mostly horseshoe-shaped.

Terrain Attributes of Earthquake- and Rainstorm-induced Landslides

To better understand the responses of landslides triggered by different drivers on landscape, the two landslide maps were overlaid onto the elevation, lithology, and slope maps to extract the means of terrain attributes for each landslide. As for elevation (Figure 6), earthquake-triggered landslides are more prone to occur at elevations between 1000 and 2000 m and >2500 m (Figure 6a.1). Within the region of earthquake intensity < VI, there is no significant signature between elevation and landslides (Figure 6a.2). In contrast, for the region of earthquake intensity ≥ VI, the landslide proportion ratios are much higher than the background as the elevation higher than 1000 m, particularly for the large landslides (Figure 6a.3). It revealed that large landslides were inclined to happen at higher elevation

Table III. Landslide comparison between Chi-Chi earthquake and Typhoon Morakot

	Chi-Chi earthquake			Typhoon Morakot		
	Mean area (km^2)	Number	R_{cir}[a]	Mean area (km^2)	Number	R_{cir}[a]
Small	0.0089	23521	0.58	0.0108	27095	0.52
Large	0.1155	1816 (7.2%)	0.43	0.2152	1357 (4.8%)	0.24
Total	0.0165	25337	0.56	0.0205	28452	0.51

[a] R_{cir} is a ratio of landslide area over the circumference which has the same perimeter as landslide.

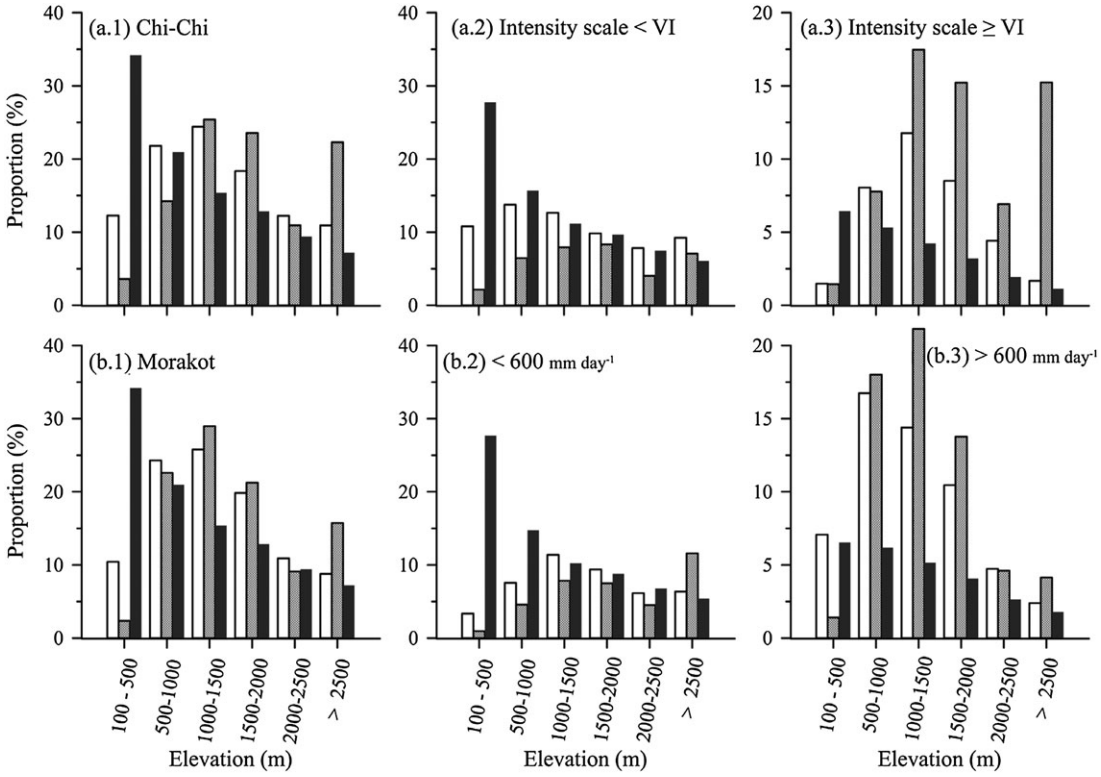

Figure 6. Landslide distributions in elevations for Chi-Chi (a.1–a.3) and Morakot (b.1–b.3). The landslide area triggered by earthquake and rainstorm were shown in (a.1) and (b.1), respectively. The landslides in the region of earthquake intensity scale < VI and maximum one-day rainfall <600 mm were shown in (a.2) and (b.2). The landslides in the region of earthquake intensity scale ≥ VI and maximum one-day rainfall >600 mm were shown in (a.3) and (b.3).

as the earthquake intensity ≥ VI, supported by Figure 4a. For typhoon-induced landslides, the daily rainfall of 600 mm day^{-1} was used as a threshold to assess if any landslide preference exhibited considering both elevation and rainfall intensity (Figures 6b.2 and 6b.3). In these figures, little landslide preference was witnessed in the condition of rainfall <600 mm day^{-1} (Figure 6b.2). However, when rainfall exceeded 600 mm day^{-1}, both small and large landslides aggregated eminently between elevations 500–2000 m (Figure 6b.3). The rainstorm-induced landslides preferentially occurred in the relatively low elevation.

For the relationship between earthquake-induced landslides and lithology (Figure 7), generally there was no significant difference of landslide proportion ratios in any lithologic unit; only the unit of argillite, quartzite, and slate had a slightly higher preference. For the unit of sandstone and slate, both small and large landslide proportion ratios were much lower than the background (Figure 7a.1), but the responses were quite different in terms of earthquake intensity. The landslide proportion ratios within the region of intensity < VI (Figure 7a.2) were less than the corresponding backgrounds, whereas they were much higher than the background for earthquake intensity ≥ VI (Figure 7a.3). The contrary results might indicate that the lithologic unit of (1) argillite, quartzite and slate, and (2) sandstone and slate could resist the small earthquake, but might suddenly collapse as shaking wave exceeds the threshold. For rainstorm-induced landslides within the region of rainfall >600 mm day^{-1}, landslides preferentially occur in the three lithologic units: (1) slate, phyllite with sandstone interbeds; (2) argillite, slate and phyllite; (3) sandstone and shale. However, there were few landslides preferentially occurred in the unit of sandstone and shale as the forcing is insufficient. This comparison showed that the erodibility of lithologic unit may be a threshold-based response with the forcing intensity.

For slopes, the gradient histograms of the entire island, small and large landslides were shown in Figure 8. Most of the slope gradients in Taiwan mountainous areas are around 20°–40°. Some area with gradient <20° in the region of elevation >100 m is located in the western plain and longitudinal valley between Eastern range and Central range. For landslides, the proportion ratios of earthquake-induced landslides are higher than the background as the slope gradient is higher than 35°, and it is particularly apparent for large landslides located in earthquake intensity scale ≥ VI. In contrast, most of the typhoon-induced landslides occurred in slopes between 25° and 45°, prominently between 30° and 35°. Meanwhile, there are only a few typhoon-induced landslides that have occurred in slopes with gradient >50°. The landslide proportional ratios of daily rainfall <600 mm day^{-1} were not significant (Figure 8

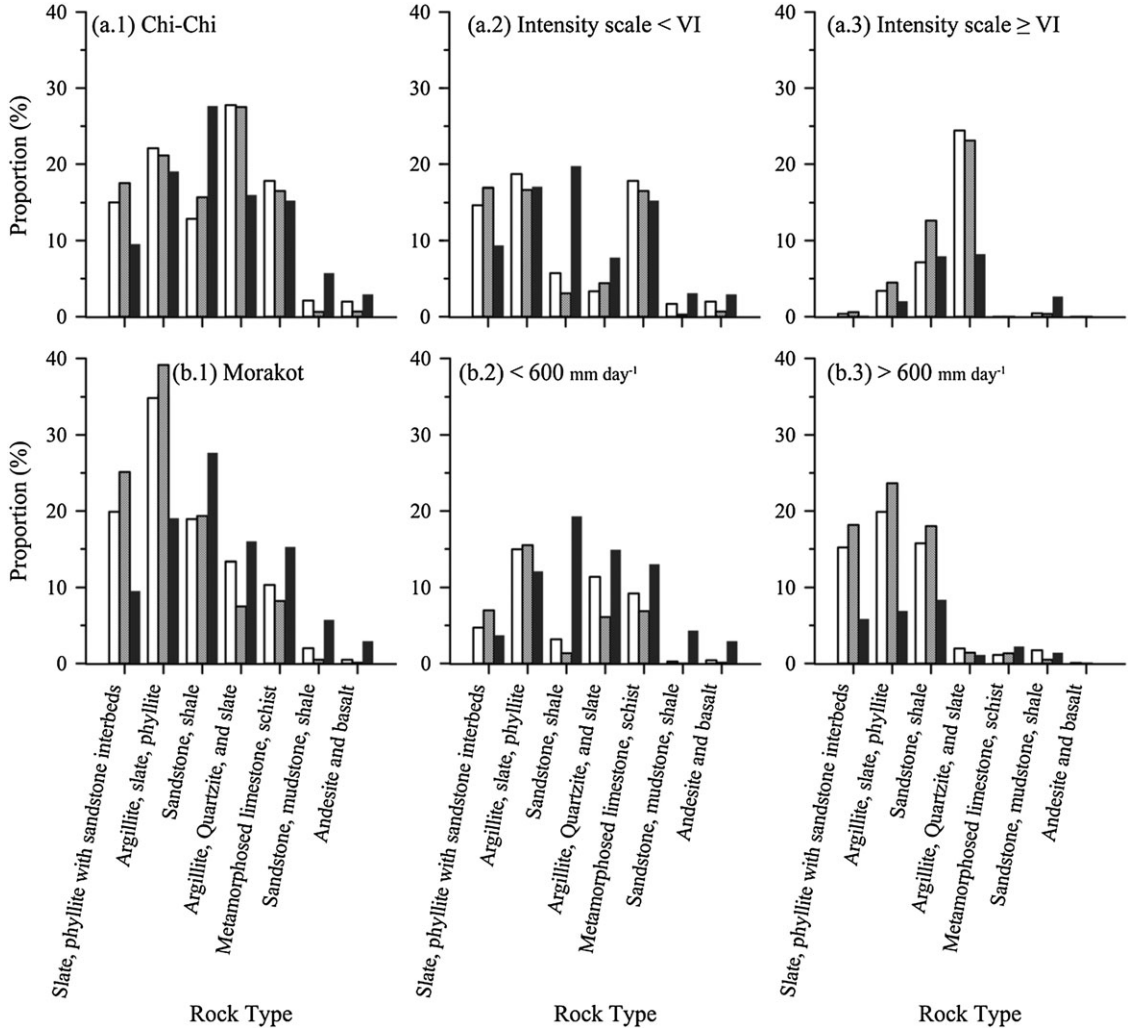

Figure 7. Landslide distributions in the regions of lithologic units for Chi-Chi (a.1–a.3) and Morakot (b.1–b.3). The whole landslides triggered by earthquake and rainstorm were shown in (a.1) and (b.1), respectively. The landslides in the region of earthquake intensity scale < VI and maximum one-day rainfall <600 mm were shown in (a.2) and (b.2). The landslides in the region of earthquake intensity scale ≥ VI and maximum one-day rainfall >600 mm were shown in (a.3) and (b.3).

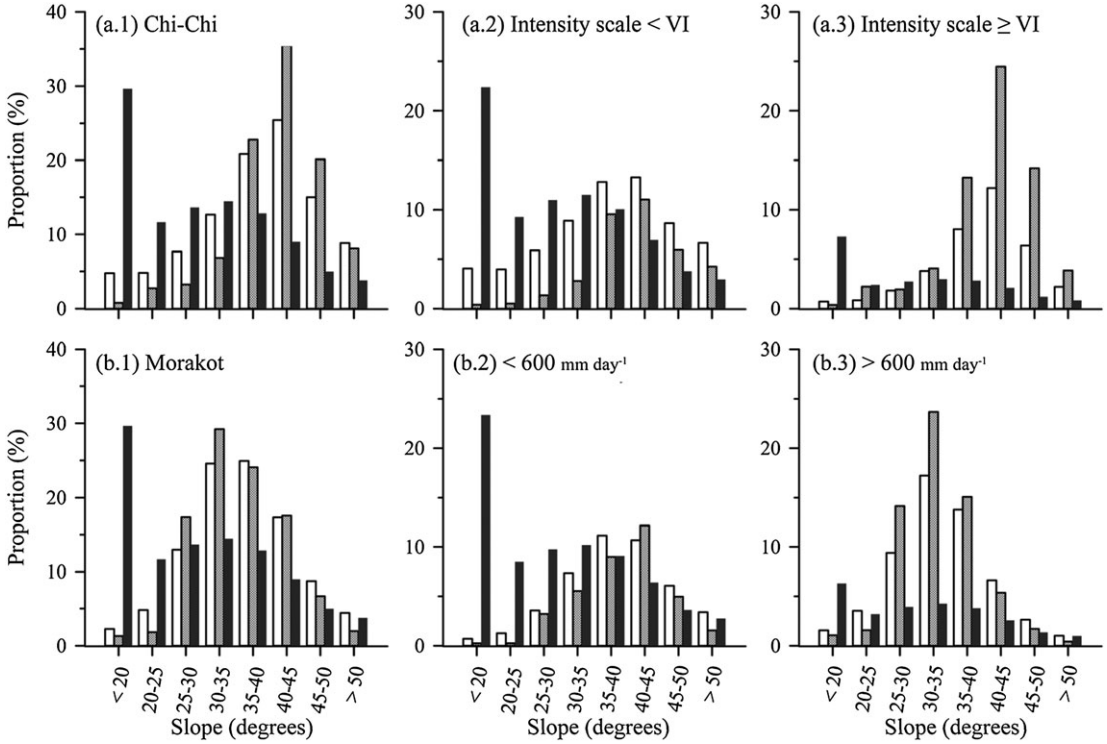

Figure 8. Landslide distributions in slope gradient for Chi-Chi (a.1–a.3) and Morakot (b.1–b.3). The landslide area triggered by earthquake and rainstorm were shown in (a.1) and (b.1), respectively. The landslides in the region of earthquake intensity scale < VI and maximum one-day rainfall <600 mm were shown in (a.2) and (b.2). The landslides in the region of earthquake intensity scale ≥ VI and maximum one-day rainfall >600 mm were shown in (a.3) and (b.3).

b.2). But the landslide proportional ratios in the region of rainfall >600 mm day^{-1} are higher than backgrounds within the slope gradient 25° and 40° (Figure 8b.3). Although down-slope mass movement is favored by steeper gradient, hillslopes too steep are adverse for the runoff accumulation which contrarily restrain landsliding by rainstorms.

The individual terrain attribute of landslide from different triggers was determined earlier; however, the coupling effects among the terrain attributes should be identified for clarification, e.g. high elevation usually correlates with steep slope. Thus, the correlation analysis for the terrain attributes was applied onto non-landslide and landslide cells induced by earthquake and rainstorm, respectively. For non-landslide, as expected, only elevation is positively correlated to slope with $\rho = 0.43$. However, there is no significant correlation between terrain attributes for earthquake-induced landslides. By contrast, for the rainstorm-triggered landslides, elevation is negatively correlated to rainfall with $\rho = -0.31$. Generally, rainfall increases with elevation and then decreases as elevation is higher than 2500 m. This negative correlation echoed what is shown in Figure 6. However, no correlation could be found between rainfall and elevation for non-landslide, likely because of the interaction of landscape and precipitation, e.g. leeward effect. Nevertheless, the correlation matrix might indicate the coupling effects among the terrain attributes are not unapparent in this study.

Location of Landslides at Hillslope Scale

Landslides by earthquake and typhoon have distinct differentiation in the earlier mentioned terrain attributes. However, elevation is not absolutely equivalent to relative locations at hillslope scale. To better understand the locations of landslides, we applied a hillslope-scale analysis to calculate the relative distances from landslide to ridge and stream in order to describe the landslide location at hillslope scale (Meunier *et al.*, 2008). In gridded DTM, the ridge cell is defined as the cell without any other upslope contributing area and the stream cell is defined as the upslope contributing area larger than 0.35 km^2 which is determined by the hillslope–stream transition plot (Huang *et al.*, 2014). Based on the determination of ridge and stream cells, the distance to ridge or stream of individual landslide could be calculated along single flow direction. Those attributes can be performed by an open-source, geospatial analysis tool: Whitebox (Lindsay, 2016). To present the landslide location at hillslope, the probability ratios (R_p) at a given normalized distances to ridge or stream is used. The equation is expressed as:

$$R_p = \frac{P\left(d_{ri,st}\right)_{ls}}{P\left(d_{ri,st}\right)_{topo}} \quad (1)$$

where $d_{ri,st}$ is the normalized distances to ridge or stream, $P(d_{ri,st})_{ls}$ is the probability of landslide cells, and $P(d_{ri,st})_{topo}$ is the probability of all cells. Similarly, to the proportional ratio, $R_p > 1$ means higher landslide preference at this relative location at hillslope scale.

The patterns of landslide locations in normalized distances to stream are illustrated in Figure 9. Earthquake-induced landslides are prone to occur between mid-slope and the toe of hillslopes. By contrast, the rainstorm-induced landslides mostly occur at the toe of hillslopes. At the top of hillslopes, landslide probability triggered by an earthquake is higher than that triggered by a typhoon (Figure 9a). In contrast, at the base of hillslopes, landslide probability triggered by a typhoon is much higher than that by an earthquake. Generally, the landslides by earthquake and typhoon differentiate in hillslope position. The pattern remains unchanged with the increase of drivers, whereas the probability increases (Figures 9b and 9c).

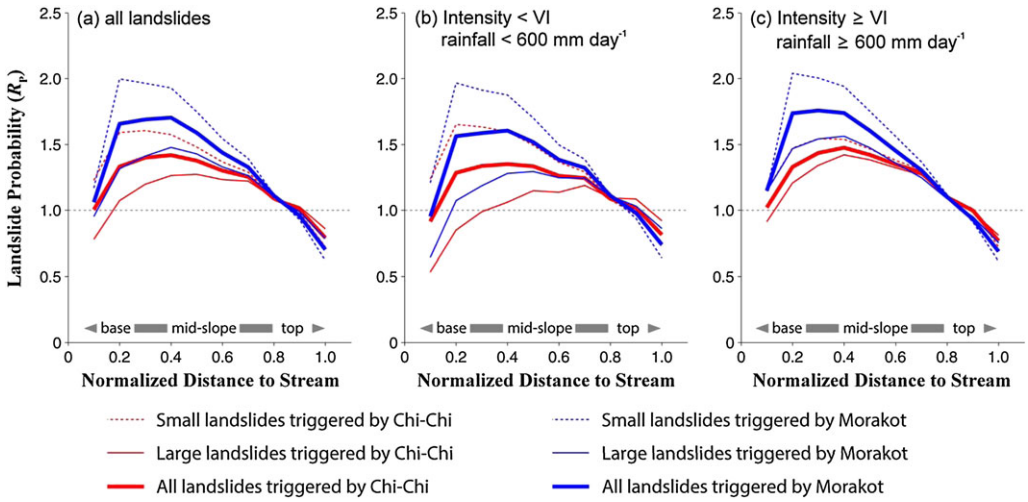

Figure 9. Landslide locations in normalized distance to stream (a). The landslides in the region of earthquake intensity scale < VI and maximum one-day rainfall <600 mm were shown in (b). The landslides in the region of earthquake intensity scale ≥ VI and maximum one-day rainfall >600 mm were shown in (c). [Colour figure can be viewed at wileyonlinelibrary.com]

Interestingly, the location of large earthquake-induced landslide moves downward with the increase of earthquake intensity.

Discussion and Remarks

Landslides induced by earthquakes and rainstorms are recognized as an important driver for shaping the landscape in montane regions (Korup, 2005b; Korup *et al.*, 2010). Moreover, the landslide-triggered sediments and above-ground biomass have been proven to play a considerable role in downstream ecosystems and carbon cycling (West *et al.*, 2011; Hilton *et al.*, 2011). In montane regions, the distinct elevation gradient which accompanies with temperature, vegetation and soil evolution also represents different states of biomass storages. Therefore, understanding the role of landslides for the earlier mentioned issues turns into the relationship between landslide density, forcing intensity and the terrain attributes of landslides induced by the two drivers. In our study, the landslide density decreased along the epicenters of the two catastrophic events, particularly for the large landslides. The landslide densities are amplified within the regions of earthquake intensity ≥ VI and rainfall >600 mm day^{-1} which can serve as a warning limit of catastrophic events for massive landslides. In fact, we also confirmed this limit by other events (Typhoon Soudelor 2015; two earthquakes with $M_w > 6$ in 2010 and 2016) and the results supported the proposed limit as well.

Conventionally the earthquake- and rainstorm-induced landslides are hypothesized to preferentially occur in upper and lower hillslopes due to amplification of seismic waves along ridgetops and greater degree of soil water saturation in slope toe, respectively (Densmore and Hovius, 2000). This hypothesis is examined and supported by Huang and Montgomery (2014) who compared the topographic locations and size of 1999 Chi-Chi earthquake- and 2001 typhoon Toraji-generated landslides in Tachia River, central Taiwan, but inconsistent results reported by Lin *et al.* (2006) and Meunier *et al.* (2008) which reported that earthquake-triggered landslides preferentially occurred on both of the lower and upper portions of hillslopes in the Choshui River basin, central Taiwan. Those studies analyzed the same catastrophic events (Chi-Chi earthquake and Typhoon Torji) in the two adjacent watersheds, but concluded conflicting results is quite interesting. In fact, most studies agreed that the earthquake-induced landslides do occur near the ridges and the rainstorm-induced ones prefer close to toes. Meunier *et al.* (2008) compared different earthquake cases and showed that earthquake-induced landslides in Taiwan are relatively preferable in mid- and low-slopes. This distinct differentiation is interpreted by seismic effect of incidence angle and inner gorge. Our result showed that the landslide signature in elevation could partly support the amplification of seismic waves and the locations of earthquake-induced landslides in mid-slope partly explained the effect of inner gorge.

The landslide area occupying 2.1–2.8% of the entire island implies limited soil accumulation and rapid vegetation recovery. For example, Huang and Montgomery (2014) found that in Tachia River there is no evidence of residual post-earthquake in the landslides during typhoon Toraji in 2001. Our previous study showed that the landslide scars only need approximately 4–6 years to be re-covered by vegetation (Huang *et al.*, 2007). For example, Lin *et al.* (2004) and Lin *et al.* (2005) investigated the vegetation recovery in central Taiwan and they found that the vegetation could be recovered ~60% over 2 years after Chi-Chi earthquake. Thus, in this study, we also could not find a significant residual effect of Chi-Chi earthquake on the Morakot landslide map (see Figure 4).

The photographs shown in Figure 10 illustrate the terrain attributes of landslides as well. Figure 10a shows numerous landslides spreading around the top of hillslopes in 99 peaks (the location shown in Figure 3a) after Chi-Chi earthquake. Before the Chi-Chi earthquake, landslides mainly occurred on the head and bottom of gullies because surface and subsurface eroded the weak-cemented conglomerate. The Chi-Chi earthquake caused rock falls and landslides on the hillslopes (Chen and Wu, 2006), and their crown extended to the ridge. Figure 10b shows a great quantity of landslides triggered by Typhoon Morakot that are located in gullies and hillslope toes in the Taimali basin, eastern Taiwan (the location also shown in Figure 3b). Groundwater seeps into the fractured bedrock during a prolonged rainfall (Chen *et al.*, 2013) and lateral erosion removed the toe of hillslopes (Stark *et al.*, 2010). Furthermore, not only the elevation and location, the shape and area of earthquake- and rainstorm-induced landslides are also different. The rainstorm-induced landslides are relatively horseshoe-shaped and large (Figure 10a), whereas the earthquake-triggered ones are round-shaped and small (Figure 10b). Other terrain attributes, such as slope, also reflect the forcing types. The earthquake-induced landslides usually

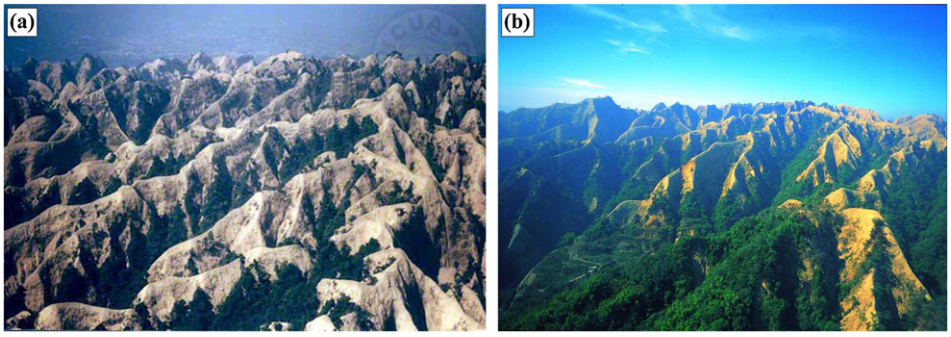

Figure 10. Landslides in 99 peaks, central Taiwan, triggered by Chi-Chi earthquake on September 21, 1999 (photograph was taken by Chyi-Tyi Lee, September 27, 1999). Most landslides occurred near the ridges and substantial material remained on hillslopes (a). Landslides, in the Taimali basin in eastern Taiwan, triggered by Typhoon Morakot on August 6–10, 2009 (photograph was taken June 22, 2011). Most landslides occurred on the downward slopes. The regolith formed the colluvium fans or transported to streams (b). [Colour figure can be viewed at wileyonlinelibrary.com]

can be found in steep gradient, particularly for the large landslides. In contrast, the typhoon-induced landslides aggregate between the gradient of 25° and 40° and preferentially occur in concave slopes. The sufficient slope length and soil depth which favor runoff accumulation may interpret the landslide preference in slopes (Kelsey, 1988; Montgomery and Dietrich, 1994). Unlike the earlier mentioned attributes, generally the lithologic response of landsliding to driving force is indistinct. As Lin *et al.* (2006) and Khazai and Sitar (2004) stated, the rainstorm- and earthquake-induced shallow landslides are not associated with lithologic units. Our results slightly agreed with this statement; however, the specific combination of forcing intensity and lithologic unit should be noted. For example, the sandstone and shale can resist landsliding as daily rainfall less than 600 mm day^{-1}; however, it becomes tenuous against daily rainfall >600 mm day^{-1}. It is similar to the lithologic unit of argillite, quartzite, and slate in the case of earthquake-induced landslides.

Finally, landslide map and their terrain attributes, in fact, record many information of the devastating events and the consequent processes. For example, landslide density can reveal the source of large earthquakes (Meunier *et al.*, 2013). We demonstrated that the terrain attributes of landslides can be justified as the first-order indexes for determination of landslide triggers. Through the landslide patterns and their terrain attributes, this retrospective approach can provide some insights to the historical and remote events for close geophysical investigation. We would state that as discussing the landscape evaluation or biogeochemical processes in landslide-dominate regions we should bear in mind that the landslide location, size, and terrain attributes varying with triggers may affect the relevant inferences that are concerned.

Acknowledgements—This study was sponsored by NSC Taiwan grants (MOST 105-2116-M-002-022, MOST 104-2119-M-018-001, MOST 105-2116-M-003-006) and National Taiwan University (105R3208). The authors would like to thank Professor Chyi-Tyi Lee for providing photograph.

References

Apaydin H, Ozturk F, Merdun H, Aziz NM. 2006. Determination of the drainage basin characteristics using vector GIS, Nord. *Hydrology* **37**: 129–142.

Chai BHT. 1972. Structure and tectonic evolution of Taiwan. *American Journal of Science* **272**: 389–422.

Chen SC, Wu CH. 2006. Slope stabilization and landslide size on Mt. 99 Peaks after Chi-Chi earthquake in Taiwan. *Environmental Geology* **50**: 623–636.

Chen RF, Chang KJ, Angelier J, Chan YC, Deffontaines B, Lee CT, Lin ML. 2006. Topographical changes revealed by high-resolution airbone LiDAR data: The 1999 Tsaoling landslide induced by the Chi-Chi earthquake. *Engineering Geology* **88**: 160–172.

Chen YC, Chang KT, Chiu YJ, Lau SM, Lee HY. 2013. Quantifying rainfall controls on catchment-scale landslide erosion in Taiwan. *Earth Surface Processes and Landforms* **38**: 372–382.

Dadson SJ, Hovious N, Chen H, Dade WB, Hsieh ML, Willett SD, Hu JC, Horng MJ, Chen MC, Stark CP, Lague D, Lin JC. 2003. Links between erosion, runoff variability and seismicity in the Taiwan orogen. *Nature* **426**: 648–651.

Dadson SJ, Hovious N, Chen H, Dade WB, Lin JC, Hsu ML, Lin CW, Horng MJ, Chen TC, Milliman J, Stark CP. 2004. Earthquake-triggered increase in sediment delivery from an active mountain belt. *Geology* **32**: 733–736.

Densmore AL, Hovius N. 2000. Topographic fingerprints of bedrock landslides. *Geology* **28**: 371–374.

Gao J, Maro J. 2010. Topographic controls on evolution of shallow landslides in pastoral Wairarapa, New Zealand, 1979–2003. *Geomorphology* **114**: 373–381.

Hilton RG, Galy A, Hovious N. 2008. Riverine particulate organic carbon from an active mountain belt: importance of landslides. *Global Biogeochemical Cycles* **22** .GB1017

Hilton RG, Meunier P, Hovious N, Bellinggham PJ, Galy A. 2011. Landslide impact on organic carbon cycling in a temperate montane forest. *Earth Surface Processes and Landforms* **36**: 1670–1679.

Ho CS. 1988. *An Introduction to the Geology of Taiwan: Explanatory Text of the Geologic Map of Taiwan*. Ministry of Economic Affairs: Taipei.

Hovius N, Stark CP, Chu HT, Lin JC. 2000. Supply and removal of sediment in a landslide-dominated mountain belt: Central Range, Taiwan. *Journal of Geology* **108**: 73–89.

Hovius N, Meunier P, Lin CW, Chen H, Chen YG, Dadson S, Horng MJ, Lines M. 2011. Prolonged seismically induced erosion and the mass balance of a large earthquake. *Earth and Planetary Science Letters* **304**: 347–355.

Huang AY-L, Montgomery DR. 2014. Topographic locations and size of earthquake- and typhoon-generated landslides, Tachi River, Taiwan. *Earth Surface Process and Landform* **39**: 414–418.

Huang JC, Kao SJ. 2006. Optimal estimator for assessing landslide model performance. *Hydrology and Earth System Sciences* **10**: 957–965.

Huang JC, Kao SJ, Hsu ML, Lin JC. 2006. Stochastic procedure to extract and to integrate landslide susceptibility maps: an example of mountainous watershed in Taiwan. *Natural Hazards and Earth System Sciences* **6**: 803–815.

Huang JC, Kao SJ, Hsu ML, Liou YA. 2007. Influence of specific contributing area algorithms on slope failure prediction in landslide modeling. *Natural Hazards and Earth System Sciences* **7**: 781–792.

Kao SJ, Milliman JD. 2008. Water and sediment discharge from small mountainous rivers, Taiwan: the roles of lithology, episodic events, and human activities. *Journal of Geology* **116**: 431–448.

Kao SJ, Huang JC, Lee TY, Liu CC, Walling DE. 2011. The changing rainfall-runoff dynamics and sediment response of small

mountainous rivers in Taiwan under a warming climate. In *Sediment Problems and Sediment Management in Asian River Basins*, Walling DE (ed). IAHS Press: Wallingford; 114–129.

Kelsey HM. 1988. Formation of inner gorges. *Catena* **15**: 433–458.

Khazai B, Sitar N. 2004. Evaluation of factors controlling earthquake-induced landslides caused by Chi-Chi earthquake and comparison with the Northridge and Loma Prieta events. *Engineering Geology* **71**: 79–95.

Korup O. 2005a. Large landslides and their effect on sediment flux in South Westland, New Zealand. *Earth Surface Processes and Landforms* **30**: 305–323.

Korup O. 2005b. Geomorphic imprint of landslides on alpine river systems, southwest New Zealand. *Earth Surface Processes and Landforms* **30**: 783–800.

Korup O, Densmore AL, Schlunegger F. 2010. The role of landslides in mountain range evolution. *Geomorphology* **120**: 77–90.

Larsen IJ, Montgomery DR, Korup O. 2010. Landslide erosion controlled by hillslope material. *Nature Geosciences* **3**: 247–251.

Lin GW, Liu SH, Lee SY, Liu CC. 2006. Impacts of the Chi-Chi earthquake on subsequent rainfall-induced landslides in central Taiwan. *Engineering Geology* **86**: 87–101.

Lin GW, Chen H, Hovious N, Horng MJ, Dadson S, Meunier P, Lines M. 2008. Effects of earthquake and cyclone sequencing on landsliding and fluvial sediment transfer in a mountain catchment. *Earth Surface Processes and Landforms* **33**: 1354–1737.

Lin WT, Chou WC, Lin CY, Huang PH, Tsai JS. 2005. Vegetation recovery monitoring and assessment at landslides caused by earthquake in central Taiwan. *Forest Ecology and Management* **210**: 55–66.

Lin CY, Lo HM, Chou WC, Lin WT. 2004. Vegetation recovery assessment at the Jou-Jou Mountain landslide area caused by the 921 Earthquake in central Taiwan. *Ecological Modeling* **176**: 75–81.

Liu CC, Shieh CL, Lin JC, Wu AM. 2011. Classification of non-vegetated areas using Formosat-2 high spatiotemporal imagery: the case of Tseng-Wen Reservoir catchment area (Taiwan). *International Journal of Remote Sensing* **32**: 8519–8540.

Lindsay JB. 2016. Whitebox GAT: a case study in geomorphometric analysis. *Computers & Geosciences* **95**. DOI:10.1016/j.cageo.2016.07.003.

Malamud BD, Turcotte DL, Guzzetti F, Reichenbach P. 2004. Landslide inventories and their statistical properties. *Earth Surface Processes and Landslides* **29**: 687–711.

Meunier P, Hovius N, Haines JA. 2008. Topographic site effects and the location of earthquake induced landslides. *Earth and Planetary Science Letters* **275**: 221–232.

Meunier P, Uchida T, Hovius N. 2013. Landslide patterns reveal the sources of large earthquakes. *Earth and Planetary Science Letters* **363**: 27–33.

Milliman JD, Lin SW, Kao SJ, Liu JP, Liu CS, Chiu JK, Lin YC. 2007. Short-term changes in seafloor character due to flood-derived hyperpycnal discharge: Typhoon Mindulle, Taiwan, July 2004. *Geology* **35**: 779–782.

Milliman J, Farnsworth KL. 2011. *River Discharge to the Coastal Ocean: A Global Synthesis*. Cambridge University Press: Cambridge.

Mondini AC, Chang KT, Yin HY. 2011. Combining multiple change detection indices for mapping landslides triggered by typhoons. *Geomorphology* **134**: 440–451.

Montgomery DR, Dietrich WE. 1994. A physically based model for the topographic control on shallow landsliding. *Water Resources Research* **30**(4): 1153–1171.

Montgomery DR, Brandon MT. 2002. Topographic controls on erosion rates in tectonically active mountain ranges. *Earth and Planetary Science Letters* **201**: 481–489.

Stark CP, Barbour JR, Hayakawa YS, Hattanji T, Hovius N, Chen H, Lin CW, Horng MJ, Xu KQ, Fukahata Y. 2010. The climatic signature of incised river meanders. *Science* **327**(5972): 1497–1501.

Teng LS. 1990. Geotectonic evolution of late Cenozoic arc-continental collision in Taiwan. *Tectonophys* **183**: 67–76.

Tsai F, Hwang JH, Chen LC, Lin TH. 2010. Post-disaster assessment of landslides in southern Taiwan after 2009 Typhoon Morakot using remote sensing and spatial analysis. *Natural Hazards and Earth System Sciences* **10**: 2179–2190.

Tsou CY, Feng ZY, Chigira M. 2011. Catastrophic landslide induced by Typhoon Morakot, Shiaolin, Taiwan. *Geomorphology* **127**: 166–178.

West AJ, Lin CW, Lin TC, Hilton RG, Liu SH, Chang CT, Lin KC, Galy A, Sparkes RB, Hovius N. 2011. Mobilization and transport of coarse woody debris to the oceans triggered by an extreme tropical storm. *Limnology and Oceanography* **56**: 77–85.

Wu CH, Chen SC. 2009. Determining landslide susceptibility in Central Taiwan from rainfall and six site factors using the analytical hierarchy process method. *Geomorphology* **112**: 190–204.